This is a preprint, the final version is subject to change, of the American Mineralogist (MSA)
Cite as Authors (Year) Title. American Mineralogist, in press.
DOI: https://doi.org/10.2138/am-2019-6800

The effect of incorporated carbonate and sodium on the IR spectra of A-, B- and AB-type carbonated apatites

Revision 2

Manuscript (6663) revised according to reviewers' comments (Aug 8, 2018) and resubmitted

Manuscript, now 6800, revised according to reviewers' comments (Jan 13, 2019)

Claude H. Yoder[1], Melissa M. Bollmeyer, Kathleen R. Stepien, and Robyn N. Dudrick

Department of Chemistry, Franklin and Marshall College, Lancaster, Pennsylvania 17603, United States

*Corresponding author 717-358-3806

Abstract

The substitution of carbonate in apatites has been voraciously explored for more than 60 years. However, the characterization of the sites of carbonate substitution in apatite by the frequently used identification method, infrared spectroscopy, is still incompletely understood. In a significant departure from previous studies, a recent IR study concluded that most of the carbonate in apatites resides in the channels, at least in apatites prepared at high temperature and pressure. A series of A- and AB-carbonated calcium and strontium apatites have been prepared by aqueous precipitation and by carbonation with CO_2 at 800 °C. The type of carbonate substitution –A- (substitution for hydroxide in the channel) or B- (substitution for phosphate)—was determined from the carbonate

[1] Corresponding author, claude.yoder@fandm.edu

asymmetric stretch (ν_3) and out-of-plane bend (ν_2) regions in the IR spectra. The IR ν_3 and ν_2 regions were analyzed by peak-fitting using both four- and six-peak models for the ν_3 region. A correlation of the band position of the high frequency A-type carbonate band frequency with weight percent carbonate was observed for the calcium apatites, whereas a correlation of the band positions of both the low and high frequency B-type carbonate bands with carbonate weight percent occurs for the strontium apatites. The high-frequency member of the A-type carbonate ν_3 region for the calcium apatites showed the greatest variation with a change in the composition (A- or B-type) of carbonate. The lower frequency observed for the A-type ν_3 band of those calcium apatites with the greatest carbonate content suggested the importance of carbonate clusters in the unit cell of highly carbonated apatites. Correlations of band frequencies with sodium content were weaker than those for carbonate, even though carbonate and sodium were correlated with each other in the calcium apatites. Analogous observations on the IR band frequencies in potassium-containing carbonated apatites, in which the potassium content is low, also suggest that carbonate content is the primary driver for the interactions that produce overlap of A-type peaks with those in the B-type region. This conclusion is further strengthened by the lack of a correlation of the frequencies of A-type carbonate in strontium apatites in which the carbonate content is low.

A comparison of the IR carbonate ν_3 region of the calcium apatites with that of apatites prepared under high pressure and temperature indicates that this region is very similar for both types of syntheses. Thus, previous conclusions about the distribution of A and B-type carbonate likely should be valid for most synthetic calcium apatites formed under a wide range of temperature and pressure conditions.

Keywords: Apatite, IR, carbonate, carbonate correlation with IR frequencies, peak-fitting, A-type carbonate, B-type carbonate

Introduction

The apatite family of minerals is said to accommodate in their structures about half of the elements of the periodic chart (Kreidler and Hummel 1970; Hughes and Rakovan 2002) and as a result the family has a variety of uses such as heavy metal remediation, ion-exchange, phosphors, and nuclear waste encapsulation. The carbonated calcium hydroxyl- member of the family bears a close resemblance to the inorganic portion of bone and teeth and is consequently used in a variety of medical orthopedic applications.

The substitution of the carbonate ion in the apatite structure is extremely facile (LeGeros 1981; Elliott 1994, 2002; Pan and Fleet 2002; Fleet 2015). Bone contains about 6 wt% carbonate and synthetic carbonated apatites have been studied since the 1950s, when LeGeros et al. (1969) found that the presence of carbonate decreased the *a*-axial unit cell length relative to that of the parent $Ca_{10}(PO_4)_6(OH)_2$, as expected for the replacement of phosphate by the smaller carbonate ion (B-type substitution). In contrast, Wallaeyes (1954), Bonel (1972) and others found that the reaction of apatite with CO_2 at high temperatures produced a carbonated apatite for which the *a*-axis increased in length and identified their product as having carbonate substituting for two hydroxides in the apatite channel (A-type substitution). Since then there have been many examples of aqueously precipitated apatites that have been identified as containing predominantly (generally greater than 90%) B-type carbonate (LeGeros 1981; Elliott 1994, 2002; Pan and Fleet 2002).

In a significant departure from previous studies, a recent IR study concluded that in apatites prepared at high temperature and pressure in the presence of sodium-containing reagents most of the carbonate resides in the channels (Fleet 2017). This careful analysis of the IR carbonate asymmetric stretch (ν_3) region and the out-of-plane bend (ν_2) region showed that the complexity of the ν_3 region is a result of the intrusion of A-type doublets on the doublet of the B-type region (Fleet 2017). This decrease in frequency of the A-type doublet may be due to the presence of sodium ion (Fleet 2017).

Sodium (and other alkali metal cations used to charge-balance the anions present in the synthesis reagents) can be incorporated into apatite during high temperature reactions of mixtures such as $CaCO_3$, Na_2CO_3, $CaHPO_4$, and $Ca(OH)_2$ (Fleet and Liu 2007) or in aqueous precipitation reactions such as the addition of $Ca(NO_3)_2$ to Na_2HPO_4 below 100 °C. These counter ions are generally thought to replace those calcium ions (Ca2) that define the apatite channels (El Feki et al. 2000; Pan and Fleet 2002). When reaction reagents contain the sodium counter ion, incorporation of Na^+ occurs as a result of co-substitution with carbonate in B-type substitution. The two most frequently encountered charge compensation schemes for B-type substitution involve: a) the loss of phosphate, calcium, and hydroxide (equation 1), and b) co-substitution of sodium with carbonate and the loss of phosphate and calcium (equation 2).

$$CO_3^{2-} = PO_4^{3-} + Ca^{2+} + OH^- \quad (1)$$

$$Na^+ + CO_3^{2-} = PO_4^{3-} + Ca^{2+} \quad (2)$$

The distinguishing features of A- and B-type carbonate in the IR spectral pattern of AB-type apatites appear to be related to the amount of incorporated Na^+(Fleet 2017; Fleet and Liu 2007)

and this may also be the case for apatites containing K^+ (Verbeeck et al. 1995). When sodium substitutes for calcium (Ca2) the charge in the channel decreases and makes A-type substitution less favorable (Barinov et al. 2008; Zyman and Tkachenko 2013). Formation of vacancies (equation (1)) has the same charge-lowering effect and consequently also affects carbonate substitution and characteristic vibrational frequencies. The effect of counter ions (and vacancies) could also depend on the location and orientation of carbonate ions, with the frequencies of A-type carbonate being more strongly affected than B-type due to the presence of Na^+ (substituting for Ca2) in the channel (Fleet and Liu 2007; Madupalli et al. 2017).

We report here our investigations of AB-apatites of the form $(A\text{-})_n(B\text{-})_m$CMApOH, where C = carbonated, M = Ca and Sr, and n and m vary to produce different series of carbonated apatites that range from pure A-type to AB-type apatites. AB-type apatites were prepared by aqueous precipitation reactions, whereas A-type products were prepared by carbonation reactions of apatite or carbonated AB-type apatite at 800 °C. A knowledge of the location of carbonate in the apatite structure is crucial to understanding the properties and biological behavior of biomaterials, particularly the possible role of the channel in ion transport and acid-base control of body fluids (Fleet 2017). In particular, our work contributes to an understanding of the extent to which the analyses that showed large amounts of A-type carbonate in high temperature/pressure sodium-bearing apatites can be extrapolated to their aqueously precipitated counterparts.

Experimental Section

Synthesis of apatite starting materials

All samples were prepared using Milli-Q deionized water and ACS reagent grade reagents with purities above 98%. ^{13}C labeled CO_2 (99% purity) was obtained from Sigma-Aldrich. Yields were >90%.

Calcium hydroxylapatite (CaApOH):

A 60 mL portion of 0.20 M $(NH_4)_2HPO_4$ was added dropwise at a rate of 1 drop/sec to 60 mL of 0.33 M $Ca(NO_3)_2 \bullet 4H_2O$ at 80°C. The ratio of calcium to phosphate followed the 5:3 stoichiometry of calcium hydroxylapatite ($Ca_5(PO_4)_3OH$). The pH was manually adjusted to 9 using 3 M NH_3 and maintained at that pH during the digestion time of 1 day at 80 °C. The precipitate was filtered through a medium porosity sintered glass filter crucible using vacuum filtration, washed 4 times with a total of 120 mL of distilled water, and dried in a vacuum oven for 3 hours at 120 °C and 5 torr.

For the aqueous synthesis of carbonated calcium hydroxylapatites (CCaApOH), 25 mL of 0.36 M $NH_4H_2PO_4$ and 25 mL of 0.60 M $Ca(NO_3)_2 \bullet 4H_2O$ were added simultaneously at a rate of 0.5 drop/sec to an amount of a 2.16 M sodium carbonate solution necessary to prepare various mole ratios of carbonate to phosphate at 80°C. A mole ratio of 1 to 1 (carbonate to phosphate) required 4.2 mL of the 2.16 M carbonate solution, which was added to 50 mL H_2O. The pH was adjusted to 9 using 3 M NH_3 during the addition and was maintained throughout the digestion time of 4 hours. The precipitate was filtered through a medium porosity sintered glass filter crucible using vacuum filtration, washed 4 times with a total of 120 mL of distilled water, and dried for 5 hours at 130°C followed by a vacuum drying for 6 hours at room temperature and 5 torr.

Strontium hydroxylapatites (SrApOH):

A 50 mL solution of 0.22 M $Sr(NO_3)_2$ was added dropwise at a rate of 1 drop/sec to 50 mL of 0.13 M $NH_4H_2PO_4$ at 90°C. The ratio of strontium to phosphate was based on the 5:3 stoichiometry of strontium hydroxylapatite ($Sr_5(PO_4)_3OH$). The pH was adjusted to 9 using 3 M NH_3 during the addition and was maintained throughout the digestion time of 2 days at 90 °C. The precipitate was filtered through a medium porosity sintered glass filter crucible using vacuum filtration, washed 4 times with a total of 120 mL of distilled water, and dried in a vacuum oven for 24 hours at room temperature and 5 torr.

Carbonated strontium hydroxylapatites (CSrApOH) were synthesized in the presence of varying concentrations of sodium by using different phosphate reagents. A 50 mL portion of 0.22 M $Sr(NO_3)_2$ and 50 mL of 0.13 M $(NH_4)_3PO_4$, NaH_2PO_4, or $Na_3PO_4 \bullet 12H_2O$ were added simultaneously at a rate of 1 drop/sec to 50 mL of 0.092 M $NaHCO_3$ or Na_2CO_3 at 90°C. The pH was adjusted to 9 during the addition using 3 M NH_3 or 3 M NaOH and was maintained throughout the digestion time of 1-2 days. The precipitate was filtered through a medium porosity sintered glass filter crucible using vacuum filtration, washed 4 times with a total of 120 mL of distilled water, and dried in a vacuum oven for 24 hours at room temperature and 5 torr.

Reaction of apatites with CO_2

About 0.1 g of the finely ground sample of apatite was placed as a thin layer in a ceramic boat and was calcined in a muffle furnace at 800°C for 7-24 hours (Wallaeys 1954). The calcined sample was placed in a quartz tube in a tube furnace. Activated (350 °C) molecular sieves were placed in 250 mL filter flasks at both ends of the tube, with the exit filter flask connected to a flow meter and

bubbler. Research grade CO_2 with less than 0.5 ppm H_2O was passed through the apparatus at a flow rate of about 0.1 L/min and the tube furnace was heated to 750-850°C for 1 day. Samples treated with ^{13}C labeled CO_2 were heated for 2 hours at 800°C under CO_2 gas using a flow rate of about 0.2 L/hour.

Characterization

Products were characterized using X-ray powder diffraction with a PANalytical X'Pert PRO Multipurpose diffractometer Theta-Theta System with Cu-K_α radiation (λ= 1.54060 Å). The samples were prepared on a cavity slide and were analyzed using the PANalytical program X'Pert Highscore Plus in a range from 5 to 70° 2θ using a step size of 0.0167 °/step and a dwell time of 3.34 s/step. Unit cell parameters were determined by referencing peaks to a PDF card for the corresponding apatite. The program UnitCell for OS X (Holland and Redfern 1997) was then used to obtain *a*- and *c*-axial lengths. Unit cell parameters were also determined by the Rietveld method using the PANalytical X'Pert Highscore Plus (version 2.3e) program. Based on repeated determinations of unit cell parameters on one compound the error is estimated to be ±0.001 Å. All products were free of impurities such as calcium or strontium phosphates ($M_3(PO_4)_2$) and calcium or strontium carbonate as indicated by XRD analyses.

A Bruker Tensor 37 IR Spectrometer with a Ge ATR mount was used to obtain the IR spectra of products using 256 scans at a resolution of 2 cm^{-1}. The uncertainty in peak positions obtained from multiple scans of the same sample is ±0.1 cm^{-1}. For all samples peak-fitting was performed on spectra not modified by smoothing or base-line correction using Thermo Scientific GRAMS/AI

Spectroscopy Software Suite. Peak fitting of the carbonate asymmetric stretch region (ν_3) was based on the model that the spectral envelope is a sum of intensity due to two to four underlying doublets, the members of which are nearly equally intense. This method is based on the assumption that both A- and B-type carbonate ions have D_{3h} or lower symmetry in the apatite structure (Tacker 2008). In the case of carbonate ions of less than D_{3h} symmetry, each structurally different ion gives rise to two asymmetric stretch and one out-of-plane bend peaks (Fleet 2015, 2017). The use of Gaussian functions for the carbonate asymmetric stretch region (ν_3) and either Gaussian or Lorentzian functions for the out of plane bend region (ν_2) accounted for at least 96% of the spectral intensity for most samples. The average standard error for the peak-fitting was 0.0011. Populations of carbonate environments (A, A', and B) were obtained from band areas assuming that the extinction coefficients for each band were the same.

Weight percent sodium was obtained using X-ray fluorescence spectroscopy (XRF) with a Panalytical PW 2404 Vacuum Spectrometer equipped with a 4 kW Rh X-ray tube. An anhydrous powder of each sample was prepared by ignition at 1200 °C, and then used to prepare a glass disc with one part anhydrous sample material and 9 parts lithium tetraborate. The uncertainty in the determination of the percentage of sodium is ± 0.02 %.

Carbonate was determined by combustion analysis using a Costech ECS4010 CHNS Analyzer and by Galbraith laboratories (Knoxville, TN), both of which involve the determination of carbonate by combustion at 950 °C. Use of oxygen to enhance combustion in the analyzer produced carbonate percentages similar to those obtained without the use of O_2. The carbonate content of similar carbonated apatites were previously determined by a combination of combustion analysis,

Raman and IR spectroscopy (Deymier et al. 2017), but for the samples in the current study the use of combustion analysis was found to be more reliable. The reported carbonate percentage for each sample was obtained from the average of two or three determinations taken from the in-house (Costech) and the Galbraith analyses. The relative error in the carbonate percentage is 5 %.

NMR spectra were obtained on an Agilent Unity 500 MHz NMR spectrometer equipped with a 3.2 mm solids probe capable of spin speeds of 24 kHz. ^{31}P and ^{13}C spectra were obtained at 202.094, and 125.500 MHz, respectively, using delay times of 30 and 100 sec, respectively. ^{31}P was referenced to calcium hydroxylapatite (Biorad) at 0.0 ppm, and ^{13}C was referenced to adamantane at 37.4 ppm.

Results

In order to study the effects of carbonate and sodium incorporation on the carbonate vibrational frequencies in apatite, three types of carbonate-containing apatites were utilized: a) A-type, prepared by reaction of uncarbonated CaApOH or SrApOH with CO_2 at 800 °C, b) AB-type calcium or strontium apatites, prepared by aqueous precipitation using sodium-containing reactants, and c) AB-type calcium or strontium apatites, prepared by carbonation of AB-type apatites (prepared by aqueous precipitation, subsequently calcined at 800 °C) with CO_2 at 800 °C.

The formation of the channel (A-type) carbonate ion in the reaction of CO_2 with apatite can be rationalized by the reaction of hydroxide, present in the channels, with the Lewis acidic CO_2:

$$CO_2 + 2\ OH^- \rightarrow {CO_3}^{2-} + H_2O$$

If all of the channel hydroxide ions were consumed to form A-type carbonate, the compound with formula $Ca_{10}(PO_4)_6CO_3$ and carbonate wt% of 5.8 would be formed. If AB-type apatite is used in

the carbonation reaction, the preliminary calcination step removes carbonate according to the equation

$$CO_3^{2-} \rightarrow CO_2 + O^{2-}$$

The "oxide" ion at the location of the former carbonate ion may react with CO_2 in the carbonation step to reform carbonate ions. In the carbonation step CO_2 may also react with hydroxide ion

$$CO_2 + O^{2-} \rightarrow CO_3^{2-}$$

in the channel. These apatites also contain varying amounts of sodium, present as a result of the substitution of calcium by sodium during the aqueous preparation of the AB-type apatite in the presence of sodium as a counter ion. The relative amounts of A- and B-type carbonate therefore depend on the amount of carbonate in the starting, AB-type apatite and on the extent of the carbonation reaction, which is controlled by the flow rate and duration of the flow of CO_2.

A-type apatites

The products of all reactions of an apatite with CO_2 were characterized by powder XRD, carbon combustion analysis, IR spectroscopy, and for some products, solid state MAS single pulse ^{13}C NMR spectroscopy. The IR spectrum of the A-type carbonated product (76P) of the reaction of CaApOH (76) with CO_2 at 800 °C contained peaks of nearly equal intensity in the carbonate asymmetric stretch (ν_3) region at 1541 and 1463 cm^{-1}. The carbonate out-of-plane bend (ν_2) region contained a single peak (879 cm-1) with a small amount of low frequency asymmetry. In the apatites prepared from ^{13}C labeled CO_2, these peaks appeared at 1508, 1419, and 854 cm^{-1}, shifted to lower frequencies as expected because of the greater mass of the ^{13}C isotope relative to that of ^{12}C. By comparison, Bonel (1972) obtained peaks for the isotopically unlabeled apatites at 1534, 1465 and 883 cm^{-1}, while Jebri et al. (2017) observed peaks at 1549,1460 and 879 cm^{-1}. The

250 frequencies of both the ν_3 and the ν_2 peaks are indicative of A-type carbonate, which has higher
251 frequencies than those of B-type carbonate (Elliott 1994; Fleet 2015, 2017).
252
253 The carbonate ν_3 region (Figure 1) of the product (16A) of the reaction of SrApOH (16) with CO_2
254 at 830°C contained peaks at 1545 and 1454 cm^{-1}, which can be assigned to an A-type doublet as
255 previously reported (1537, 1451 cm^{-1}) by Bonel (1972). In the ν_2 region a peak at 877 cm^{-1}
256 corresponds to the peak at 874 cm^{-1} reported by Bonel (1972). In the IR spectrum of strontium
257 hydroxylapatite prepared using ^{13}C labeled CO_2 the peak positions were 1508, 1415, and 851
258 cm^{1}.
259 **Figure 1**
260
261 The unit cell parameters obtained for products of the reaction of MApOH (M = Ca or Sr) with CO_2
262 at 800 °C (Table 1) provide additional assurance of A-type substitution. The increase in the *a*-
263 axial length of the A-type products relative to the axial length for the un-carbonated parent has
264 been recognized as a fundamental characteristic of A-type substitution since the 1950s (Elliott
265 1994).
266
267 **Table 1.**
268 **AB-type apatites**
269 In the aqueous addition reactions used to prepare the AB-type apatites, co-substitution of sodium
270 and carbonate ions occurred to give, on average, 0.6 mole of Na per mole of incorporated
271 carbonate ($r^2 = 0.95$). These carbonated apatites were subjected to calcination at 800 °C, and
272 subsequently to reaction with CO_2. Thus, the products are AB-type apatites, which contain

varying amounts of sodium, present as a result of the replacement of some Ca^{2+} ions by Na^{+} ions during the aqueous preparation of the B-type apatite.

The IR spectrum of a product of this oxide/hydroxide-directed carbonation can be seen in Figure 2, which shows the carbonate ν_3 and ν_2 regions, as well as the phosphate ν_3 region of the starting carbonated apatite (32) and the product (32P) of the reaction with CO_2. Both the ν_3 and ν_2 carbonate regions show that (32) appears (top spectrum) to contain mostly B-type carbonate, which was removed by calcination leaving oxide in its place (middle spectrum). During carbonation the CO_2 with both oxide ions, which essentially reproduces the B-type carbonate of the starting apatite, and with hydroxide ions in the channel (bottom spectrum).

The small high frequency peak at 1543 cm^{-1} in the product (32P) can be attributed to A-type carbonate because of its position relative to that of the A-type carbonate in (76P) shown in Figure 3 (a) middle panel. The increase in the intensity of the high frequency limb of the B-type doublet (1452 cm^{-1}) can be ascribed to the intrusion of the low frequency limb of the A-type doublet. The presence of only a small amount of A-type carbonate can be attributed to the relatively short duration of the reaction; that is, there was insufficient time for the CO_2 to produce additional channel carbonate ions.

Like the ν_3 region, the ν_2 region of the carbonated product can be rationalized as a combination of a small amount of A-CCaApOH with a majority of B-CCaApOH. The 874 cm^{-1} frequency of the major peak of the product confirms the dominance of B-type carbonate (Fleet 2015, 2017).

Figure 2

296

297 **IR band-fitting**

298 A careful analysis of the carbonate asymmetric stretch (ν_3) and out-of-plane bend (ν_2) regions
299 requires the fitting of bands to an envelope of spectral intensity that extends from about 1560 to
300 1370 cm^{-1} (ν_3) and from about 880 to 840 cm^{-1} (ν_2) for calcium apatites. Two models were used
301 for band-fitting of the calcium apatites: for both models the number of bands in the ν_3 region was
302 twice the number of bands used in the ν_2 region. Because the ν_2 region is relatively free of other
303 peaks it generally does not require baseline correction and is most definitive of the type of
304 carbonate substitution (Fleet 2015). For all of the AB-calcium apatites in this study, over 95% of
305 the spectral intensity in both regions was accounted for by Gaussian functions. In the ν_2 region
306 one band was present in the A-carbonate region of 880 – 875 cm^{-1}, and one band appeared in the
307 B-carbonate region of 874-870 cm^{-1} (Fleet 2015, 2017). In the ν_3 region each carbonate ion in a
308 different environment appears as a doublet of nearly equally intense bands.

309

310 In the four-band model (see Figure 3 (a)), the carbonate ν_3 region was accounted for with four
311 bands—two A-type and two B-type. In the second model (see Figure 3 (b)) six bands were
312 utilized in the ν_3 region. The six-band model has a number of advantages over the four- band
313 model: a) it accounts for a greater percentage of the spectral intensity, b) it accommodates the use
314 of doublet pairs of nearly equal areas, and c) the separation of the bands in each doublet ($\Delta\nu$) for A
315 and B bands are more comparable to A and B assignments in the literature (Tacker 2008), where
316 $\Delta\nu(A) > \Delta\nu(B)$. The six-band model has the disadvantage of introducing two bands, labeled A' in
317 the ν_3 region, that have no simple correspondence to most literature band assignments. These two
318 A' bands are present in the fitted ν_3 region of the IR spectra of every apatite in this study and are of

similar width and frequency (ca. 1400 and 1500 cm^{-1}) to bands 2 and 6 in the band-fitted ν_3 region of LM005 (Fleet 2017). Fleet (2017) assigned these bands to members of doublets attributed to A-type carbonates in different channel environments (Fleet 2017). The 6-band model requires the use of three bands in the ν_2 region, two of which are believed to correspond to two A-type carbonate environments and one to B-type carbonate. Because of the change in population of the A' band with carbonate/sodium incorporation we attribute the A' band to carbonate in channels in which a calcium ion has been replaced by either a sodium ion or a vacancy. The band at 866 cm^{-1} in the ν_2 region could also be assigned to labile carbonate (Rey et al. 1989).

Figure 3, with its vertical stacks of three panels, shows the relationship of the bands in the ν_3 region of essentially 100 % A-type carbonate apatite (76P) (middle panel) to the fitted Gaussian bands of the same region for apatite (82P) (bottom panel) that resulted from the reaction of AB-type aqueously precipitated apatite (82) (top panel) with CO_2. Because the ν_2 region contains bands at 879 and 872 cm^{-1}, strongly suggestive of A and B-type carbonates, respectively, the ν_3 region of 82P should be described by a total of four Gaussian bands. Both the four- and six-band models for fitting the ν_3 region of apatites (82) and (82P) are shown in Figure 3. Figure 4 shows the three-band interpretation of the ν_2 region of (82). consistent with the six-band fitting for the ν_3 region.

Figure 3

Figure 4

The process of tracing the A- and B-type bands through band-fitting is also shown (Figure 5) for an apatite containing a greater percentage of carbonate. The aqueously precipitated apatite (33)

contains 19.8 wt% carbonate and 3.9 wt% sodium. Band-fitting for the ν_3 carbonate region of (33) is shown in the top panel of figure 5, using a six-band model. The bands at 1528 and 1470 cm^{-1} represent A-type bands, whereas the B-type doublet appears at 1444 and 1413 cm^{-1}. The B-type bands mirror two bands in (33P) at 1443 and 1409 cm^{-1}. The A-type bands of the product appear at 1532 and 1458 cm^{-1}. Band frequencies are given in Table 2.

Figure 5

Table 2

The calcium and strontium apatites differ by the presence of a greater amount of A-type carbonate in the carbonated strontium apatites (Weidner et al. 2015). Analysis of the strontium apatite band areas in the ν_2 region reveals that A-type carbonate constitutes over half of the total peak areas in some compounds, consistent with the increase in a-axis length with carbonate substitution (Table 1) (Weidner et al. 2015; Jebri et al. 2012). An example of the carbonation product (44P) of a strontium apatite (44) containing 3.8 wt% carbonate and 0.3 wt% sodium is shown in Figure 6. Although the product contains considerable A-type carbonate, the B-type carbonate region is still visible in the ν_3 region. The A-type bands appear at 1544 and 1452 cm^{-1} with the B-type bands at 1427 and 1397 cm^{-1}. The carbonate composition of the product consists of 78% A-type according to an analysis of the areas of the constituent ν_3 peaks (82 % A-type based on ν_2). Band frequencies for the carbonated strontium apatites are given in Table 3.

Table 3

Figure 6

Discussion

Many apatites contain an alkali metal cation M^+ that has substituted for calcium in the process of compensating for the local charge imbalance that occurs during substitution of carbonate for phosphate in apatites precipitated in aqueous solution. Although M^+ may be a counter ion in, for example, a phosphate reagent (e.g., Na_3PO_4) used in the synthesis of apatite, it is not necessarily incorporated into the apatite; that incorporation depends in part upon its stability in the apatite structure. For example, the use of Rb_3PO_4 as a reagent in the synthesis of a sulfated apatite results in very small amounts of incorporated Rb^+ in the product apatite due to the large size of the ion (Tran et al. 2017). However, the use of sodium reagents in aqueous carbonate substitution reactions generally results in sodium-containing products, such as $Ca_9Na(PO_4)_5(CO_3)(OH)_2$, probably because of the energetically favorable exchange of sodium for calcium (De Maeyer, et al. 1996). In this study sodium was introduced by co-substitution with carbonate utilizing sodium-containing reagents.

The frequencies of the carbonate (ν_3) asymmetric stretch modes of carbonated apatites are influenced by a variety of factors such as:

a) the local environment of carbonate, including electrostatic interactions with cations and other anions. These interactions produce the higher asymmetric stretch and out-of-plane bend frequencies for A-type carbonate relative to B-type carbonate. Electrostatic interactions also affect carbonate substituted for phosphate, but are weaker due to the greater separation of carbonate from the channel cations.

b) the number and proximity of other carbonate ions. If the concentration of carbonate is low, it is statistically likely that carbonate ions are randomly scattered throughout unit cells over the

386 entire apatite crystallite. At higher concentrations, there is a higher probability of forming
387 clusters of carbonate ions, thereby producing greater inter-carbonate interactions.
388
389 c) The presence of Na^+ ions (and other +1 counter ions), as substitutions for Ca^{2+} in the channel
390 wall lowers the charge surrounding carbonate in the channel, thereby potentially favoring
391 substitution of carbonate for phosphate (Zyman and Tkachenko 2013; Yoder et al. 2016). The
392 decrease in charge within the channels is also experienced by B-type carbonate ions. Because
393 substitution of M^+ for Ca^{2+} usually occurs during co-substitution of carbonate it is likely that
394 the distance between the substituted carbonate and the M^+ ions is relatively small (within the
395 same or neighbor unit cells), potentially making the effect of Na^+ on vibrational frequencies
396 significant. It is also likely that A- and B-type carbonate and Na^+ are physically coupled, an
397 interaction supported by X-ray diffraction data (Fleet 2015). Because of the smaller distance
398 between an A-type carbonate ion and a Na^+ replacement for a channel calcium ion, the effect is
399 greater for A-type carbonate (Fleet 2015). In the IR spectra of sodium-containing apatites
400 prepared at high temperature and pressure the high-frequency band of the type-A carbonate is
401 shifted from its frequency of ca. 1544 cm^{-1} in sodium-free carbonated apatites (synthesized at
402 high temperature and pressure) to below 1500 cm^{-1} where it is combined with, and
403 indistinguishable from, B-type peaks (Fleet and Liu 2007; Fleet 2015, 2017).
404
405 **Correlations of peak frequencies**
406 Tables 2 and 3 contain the carbonate asymmetric stretching (ν_3) frequencies for all carbonated
407 calcium and strontium apatites in this study. A comparison of both A- and B-type carbonate
408 asymmetric stretch frequencies for the calcium apatites with both low and high amounts of A-type

409 carbonate (Table 4) shows that the amount of A-type carbonate does not much affect the B-type
410 carbonate stretch frequencies, which vary only by 9 cm^{-1} for both the high- and low-frequency
411 members. The A-type frequencies, on the other hand, vary by 16 cm^{-1} (high frequency member)
412 and 14 cm^{-1} (low frequency member). Table 2 shows a variation of 26 and 22 cm^{-1} in the high-
413 and low-frequency A-type bands and 12 and 11 cm^{-1} in the high- and the low-frequency B-type
414 bands. The position of the high-frequency member of the A-type carbonate ν_3 region therefore has
415 the greatest variation with change in the proportion of A- and B-type carbonate ions (cf. Madupalli
416 et al. 2017).

417 **Table 4**

418

419 The carbonate frequencies also appear to be related to the total amount of carbonate: lower values
420 for the frequencies of the high-frequency member of the A-type doublet are shown by the calcium
421 apatites with the largest amount of carbonate (Table 4). This observation suggests that there may
422 be a correlation between the extent of carbonation and the A-type frequencies. Figure 7 shows the
423 relationship between the high frequency member of the A-type doublet for the calcium apatites and
424 the percent carbonate in the apatite with two points omitted. Although the relationship is clear, the
425 point-by-point correlation is only moderate ($r^2 = 0.69$), but with two points omitted the correlation
426 improves to $r^2 = 0.86$. A very similar correlation was obtained with band frequencies obtained
427 using the four-band model.

428

429 Scatter in the correlations can be attributed to errors in the carbonate content (relative error = 5%),
430 errors in band fitting (which depend on the model used, the number and types of bands employed,
431 and the quality of the fit to the spectral data), spectral processing (the use of smoothing and/or base

line correction), and the resolution and quality of the original spectra. In our experience the principal source of error is likely to reside in the carbonate wt%, and this is shown in the error bars in Figure 7.

Figure 7

Because wt% CO_3 and wt% Na are correlated in the apatite samples, a correlation of the frequencies for the high frequency type-A band relative to wt% Na was also expected, but is weaker than that for carbonate. Correlations of the other bands (low-frequency A-type, high- and low-frequency B-type) with wt% carbonate (and wt% Na) are considerably weaker.

Carbonate clusters

The highly carbonated calcium apatites have an average of over two carbonate ions per unit cell, which could lead to local concentrations of more than four carbonate ions in two adjacent unit cells. These clusters would also include counter ions and/or vacancies and could involve special accommodation or coupling (Fleet 2015) of carbonate ions. The clusters could produce a large effect on the frequencies of local carbonate ions, especially those in the channels.

Strontium apatite correlations

Surprisingly, the frequencies of the A-type carbonate bands in the ν_3 region of the IR spectra of the strontium apatites are not well correlated with either wt% CO_3 or wt% Na, while the frequencies of both the high- (Figure 8, $r^2 = 0.89$) and low-frequency B-type ($r^2 = 0.75$) bands give correlations showing an increase in IR vibrational frequency with an increase in wt% CO_3. The low-frequency B-type frequencies also show a correlation with wt% Na ($r^2 = 0.77$), and, like the carbonate correlations, shown an increase in frequency with an increase in wt% Na.

Figure 8

The difference in the correlations of the A-type frequencies with respect to carbonate and sodium concentrations found for the calcium and strontium apatites can be attributed to three factors: the lower degree of carbonate saturation during synthesis of the Sr apatites, the larger size of the channels in the Sr apatites, and the lower probability of carbonate clusters in the Sr apatites. During the synthesis using the reagents and conditions specified in the Experimental Section, up to approximately 20% carbonate can be incorporated into calcium apatite, but only 7% carbonate in strontium hydroxylapatite (if more carbonate is present, strontium carbonate is formed). The smaller number of carbonate ions per unit cell for the strontium apatites, makes the probability of high carbonate clusters less likely. Finally, the larger size (Shannon 1976) of the strontium ion (1.18 Å) than the calcium ion (1.00 Å) results in a greater distance between the carbonate ion (or sodium ion) and the strontium ions in the channel and leads to a smaller effect on the vibrational frequencies.

The stronger correlation of carbonate asymmetric stretch frequencies with carbonate concentration, relative to sodium concentration, suggests that the vibrational frequencies may be affected primarily by carbonate content. The possibility of the influence of carbonate/Na clusters on the A-type vibrational frequencies seems particularly likely for highly carbonated calcium apatites. The lack of significant correlations between wt% carbonate and the high frequency A-type bands in the strontium apatites may be a result of the larger channel distances and the smaller number of carbonate ions per unit cell (and smaller probability of carbonate/sodium clusters) in these compounds.

The apatites explored in this study accommodate carbonate mainly by co-substitution of sodium. Our attempts to synthesize highly carbonated apatites in the presence of potassium ions indicate that these products contain only a small percentage of potassium and a maximum of 14 wt% carbonate (the same mole ratios in the presence of Na^+ produced 20 wt% carbonate). The ν_3 region of the more highly carbonated apatites containing a ten times smaller number of moles of potassium than their sodium homologs also showed a decrease in the frequency of the highest frequency A-type peaks relative to that frequency in less carbonated apatites. Hence, it is likely that the extent of carbonation, rather than the amount of counter ion, controls the change in vibrational frequencies.

Implications

Although other charge balance mechanisms for B-type carbonate incorporation in apatites may not show precisely the same effects on vibrational frequencies (Vignoles et al. 1988), sodium-containing apatites prepared by solid state reaction at high temperature and pressure have a similar pattern of vibrational frequencies to the ones in this study. Figure 9 compares the carbonate ν_3 region of a sodium-containing apatite (LM005) prepared at high temperature and pressure (Fleet 2017) with the same region of the IR spectra of two apatites from this study (77 and 77P). The higher intensity of the middle peak at ca. 1450 cm^{-1} in LM005, relative to those of the apatite starting materials (such as (77)), which contain mostly B-type apatite, is a result of the greater percentage of A-type carbonate, characteristic of reactions at high temperature (Yoder et al. 2016). Figure 9c shows that the high temperature/pressure apatite is closer in overall appearance to

products containing a greater percentage of A-type carbonate (such as (77P)), as well as human enamel (Fleet and Liu 2007). Fleet's demonstration of higher percentages of channel carbonate in apatites prepared at high temperature and pressure depended heavily on the deconvolution of the IR carbonate ν_3 region of sample LM005. It appears to us likely that these observations (Fleet 2017) can be extrapolated to synthetic apatites prepared by aqueous precipitation and probably also to bioapatites. The "B-type appearance" of the ν_3 carbonate region of the IR spectra of apatites with greater carbonate and sodium concentrations is a result of the decrease in frequency of the high frequency A-type band and a change in the population of the A- and A'-type bands.

Finally, we return to the interpretation of the A' bands in the fitted ν_3 and ν_2 carbonate regions of the IR spectra of the calcium hydroxylapatites (Table 3). If our interpretation of the A' sites as a second channel environment is correct, then all of the calcium apatites prepared in this study have a greater percentage of channel carbonate than that reported in the vast majority of the apatite literature. This conclusion is also borne out by our three-band interpretation of the ν_2 carbonate region of (82) (Figure 4) where the third band at 867 cm^{-1} could alternatively be assigned to another carbonate species such as labile carbonate (Rey et al. 1989). This region is unchanged after heating to 600 °C (24 h) making labile carbonate unlikely. In the absence of a deconvolution model that would eliminate the need for a second A-type environment we propose that additional channel sites be considered for carbonated calcium apatites prepared in aqueous solution.

Figure 9

Acknowledgements

The authors are indebted to Jill Pasteris (Department of Earth and Planetary Sciences, Washington University, St Louis, MO) for Raman spectra and helpful discussions, Stanley and Karen

524 Mertzman and Emily Wilson (Department of Earth and Environment, Franklin and Marshall
525 College) for analytical work, the Camille and Henry Dreyfus Foundation for a Senior Scientist
526 Mentor award (CHY), and the Lucille and William Hackman Program and the Yoder Student
527 Research Endowment at Franklin & Marshall College for funding.

528

529

530 **References**

531 Barinov, S.M., Fadeeva, I.V., Ferro, D., Rau, J.V., Cesaro, S.N., Komlev, V.S., and Fomin, A.S.
532 (2008) Stabilization of carbonate hydroxyapatite by isomorphic substitutions of sodium for
533 calcium, Russian Journal of Inorganic Chemistry, 53, 164-168.

534

535 Bonel, G. (1972) Contribution to the study of the carbonation of apatite. 1. Synthesis and
536 physicochemical properties of type A carbonated apatites. Annales de Chimie France, 7, 65-87.

537

538 De Maeyer, E.A.P., Verbeeck, R.M.H., and Pieters, I.Y. (1996) Carbonate and alkalimetal
539 incorporation in calciumhydroxyapatite. Trends in Inorganic Chemistry, 4, 157-171.

540

541 Deymier, A.C., Nair, A.K., Depalie, B., Qin, Z., Arcot, K., Drouet, C., Yoder, C.H., Buehler, M.J.
542 Thomopoulos, S., Genin, G.M., and Pasteris, J.D. (2017) Protein-free formation of bone-like
543 apatite: New insights into the key role of carbonation. Biomaterials, 127, 75-88.

544

545 El Feki, H., Savariault, J.M., Salah, A.B., and Jemal, M. (2000) Sodium and carbonate distribution
546 in substituted calcium hydroxyapatite. Solid State Sciences, 2, 577-586.

Elliott, J.C. (1994) Structure and chemistry of the apatites and other calcium orthophosphates. Studies in Inorganic Chemistry 18, 389 p. Elsevier, Amsterdam.

Elliott, J.C. (2002) Calcium Phosphate Biominerals, Reviews in Mineralogy and Geochemistry, 48, 427-455.

Fleet, M.E. and Liu, X. (2007) Coupled substitution of type A and B carbonate in sodium-bearing apatite. Biomaterials, 28, 916-926.

Fleet, M.E. (2015) Carbonated hydroxyapatite: Materials, synthesis, and application. CRC Press, Fl (Taylor and Francis Group).

Fleet, M. (2017) Infrared spectra of carbonate apatites: Evidence for a connection between bone mineral and body fluids. American Mineralogist, 102, 149-157.

Holland, T.J.B., and Redfern, S.A.T., (1997) Unit cell refinement from powder diffraction data: the use of regression diagnostics. Mineralogical Magazine, 61, 65-77.

Hughes, J.M., and Rakovan, J. (2002) The crystal structure of apatite, $Ca_5(PO_4)_3(F,OH,Cl)$, Reviews in Mineralogy and Geochemistry, 48, 1-12.

569 Jebri, S. Boughzala, H., Bechrifa, A., and Jemal, M. (2012) Structural analysis and
570 thermochemistry of "A" type phosphostrontium carbonate hydroxyapatites. Journal of Thermal
571 Analysis and Calorimetry, 107, 963-972.
572
573 Jebri, S. Boughzala, H., Bechrifa, A., and Jemal, M. (2013) Rietveld structural refinement of "A"
574 type phosphostrontium carbonate hydroxyapatites. Powder Diffraction, 28, S409-S424.
575
576 Jebri, S., Khattech, I., and Jemal, M. (2017) Standard enthalpy, entropy and Gibbs free energy of
577 formation of "A" type carbonate phosphocalcium hydroxyapatites. Journal of Chemical.
578 Thermodynamics, 106, 84-94.
579
580 Kazin, P.E., Zykin, M.A., Dinnebier, R.E., Magdysyuk, O.V., Tretyakov, Yu.D., and Jansen, M.
581 (2012) An unprecedented process of peroxide ion formation and its localization in the crystal
582 structure of strontium peroxy-hydroxyapatite Sr10 (P O4)6 (O2) x (O H)(2-2x). Zeitschrift fuer
583 Anorganische und Allgemeine Chemie, 638, 909-919.
584
585 Kreidler, E.R., and Hummel, F.A. (1970) The crystal chemistry of apatite structure fields of fluor-
586 and chlorapatite. American Mineralogist, 55, 170-184.
587
588
589 LeGeros, R.Z., Trautz, O.R., Klein, E., and LeGeros, J.P. (1969) Two types of carbonate
590 substitution in the apatite structure. Experientia, 25, 5-7.
591

LeGeros, R. Z., (1981) Apatites in biological systems. Progress in Crystal Growth and Characterization, 4, 1-46.

Madupalli, H., Pavan, B., and Tecklenburg, M.M.J. (2017) Carbonate substitution in the mineral component of bone: discriminating the structural changes, simultaneously imposed by carbonate in A and B sites of apatite. Journal of Solid State Chemistry, 255, 27-33.

Pan, Y., and Fleet, M.E. (2002) Compositions of the apatite-group minerals: substitution mechanisms and controlling factors. Reviews in Mineralogy and Geochemistry, 48, 13-49.

Rey, C., Collins, B., Goechi, T., Dikson, J.R., and Glimcher, M.J. (1989) The carbonate environment in bone mineral: A resolution-enhanced Fourier transform infrared spectroscopy study. Calcified Tissue International, 45, 157-164.

Shannon, R.D. (1976) Revised effective radii and systematic studies of interatomic distances in halids and chalcogenides. Acta Crystallographica Section A, 32, 751-767.

Sudarsanan, K., and Young, R.A. (1969) Significant precision in crystal structural details: Holly Springs hydroxyapatite. Acta Crystallographica, Section B: Structural Crystallography and Crystal Chemistry, 25, 1534-1543.

Tacker, R. C. (2008) Carbonate in igneous and metamorphic fluorapatite: Two type A and two type B substitutions. American Mineralogist, 93, 168-176.

Tran, L.K., Stepien, K.R., Bollmeyer, M.M., and Yoder, C.H. (2017) Substitution of sulfate in apatite. American Mineralogist, 102, 1971-1976.

Verbeeck, R. M.H., De Maeyer, E.A.P., and Driessens, F.C.M. (1995) Stoichiometry of potassium- and carbonate-containing apatites synthesized by solid state reactions. Inorganic Chemistry, 34, 2084-2088.

Vignoles, M., Bonel,G., Holcomb, D.W., and Young, R.A. (1988) Influence of preparation conditions on the composition of type B carbonated hydroxyapatite and on the location of the carbonate ions. Calcified Tissue International, 43, 33-40.

Wallaeys, R. (1954) Study of carbonate apatite obtained by synthesis in the solid state. Silicon, sulphur, phosphates. Colloguium of the International Union of Pure and Applied Chemistry, Munster, Verlag Chemie, Weinheim, Germany, 183-190.

Weidner, V.L., Carney, M.C., Schermerhorn, D.V., Pasteris, J.D., and Yoder, C.H. (2015) A-type substitution in carbonated strontium fluor-, chlor- and hydroxylapatites. Mineralogical Magazine, 79, 399-412.

Yoder, C.H., Landes, N.T., Tran, L.K., Smith, A.K., and Pasteris, J.D. (2016) The relative stabilities of A- and B-type carbonate substitution in apatites synthesized in aqueous solution. Mineralogical Magazine, 80, 977-983.

Zyman, Z.Z., and Tkachenko, M.V. (2013) Sodium-carbonate co-substituted hydroxyapatite ceramics. Processing and Application of Ceramics. 7, 153-157.

Figure Captions

Figure 1. The carbonate asymmetric stretch (ν_3), phosphate asymmetric phosphate stretch (ν_3), and carbonate out-of-plane bend (ν_2) regions of the IR spectrum of A-type CSrApOH (16P). The absence of an OH peak at ca. 3570 cm^{-1} (not shown) suggests that carbonation of the channel eliminated most of the OH^-. The wt% carbonate for the compound is 3.0, whereas a strontium apatite with complete substitution of carbonate for hydroxide ($Sr_{10}(PO_4)_6CO_3$) would contain 4.0 wt% carbonate.

Figure 2. IR spectra of carbonated apatite (32), calcined (32), and (32P). Top spectrum: carbonated apatite (32) prepared by aqueous precipitation using NaH_2PO_4. Middle spectrum: the apatite after calcination. Bottom spectrum: the apatite (32P) obtained by carbonation (CO_2) of the calcined apatite.

Figure 3. (a) Four-band fit and (b) six-band fit of the ν_3 carbonate region of the IR spectra of AB-type CCaApOH (82) and the product (82P) of the reaction of (82) with CO_2 at 800 °C. Top panel: Fit for AB-type CCaApOH (82). Middle panel: Bands for pure A-type CCaApOH (76P). Bottom panel: Fit for the product (82P) of the reaction of (82) with CO_2 at 800 °C. Dotted vertical lines at 1542 and 1461 cm^{-1} are band positions for A-type (76P), while lines at 1450 and 1416 cm^{-1} correspond to B-type bands. Dotted spectral lines are the experimental spectrum, whereas solid lines correspond to the "spectrum" created by peak fitting.

661

662 **Figure 4**. The carbonate ν_2 region of the IR spectrum of CCaApOH (82) using a
663 three-band model for band–fitting. The bands occur at 880 cm^{-1} (A-type), 873
664 cm^{-1} (B-type) and 867 cm^{-1} (A'-type or labile carbonate). Dotted spectral lines
665 are the experimental spectrum, whereas solid lines correspond to the "spectrum"
666 created by peak fitting.

667

668 **Figure 5.** Six-band fit of the carbonate ν_3 region of the IR spectrum for AB-type CCaApOH (33)
669 and the product (33P) of the reaction of (33) with CO_2 at 800°C. Top panel: Six-band fit for
670 CCaApOH (33). Middle panel: Peaks for pure A-type CCaApOH (76P). Bottom panel: Six-band
671 fit for the product (33P) of the reaction of (33) with CO_2 at 800 °C. Dotted lines at 1542 and 1461
672 cm^{-1} are band positions for A-type (76P), while lines at 1444 and 1412 cm^{-1} correspond to B-type
673 bands. Dotted spectral lines are the experimental spectrum, whereas solid lines correspond to the
674 "spectrum" created by peak fitting.

675

676 **Figure 6.** The carbonate ν_3 region of the IR spectrum of the strontium apatite (44P), containing 3.8
677 % carbonate and 0.3 % Na. Dotted spectral lines are the experimental spectrum, whereas solid
678 lines correspond to the "spectrum" created by peak fitting.

679

680 **Figure 7.** Least squares correlation of the IR carbonate frequencies (ν_3) for the high frequency
681 member of the A-type bands of AB-CCaApOH relative to wt% CO_3. Point for (41) omitted.

682

683 **Figure 8.** The IR carbonate frequencies (ν_3) for the high frequency member of the B-type peaks of
684 AB-CSrApOH relative to wt% CO_3. Points for (44) and (42A) omitted.
685
686 **Figure 9.** Comparison of IR carbonate spectral regions (ν_3) of AB-CCaApOH (77) and (77P)
687 from this study to AB-CCaApOH (LM005) prepared at high temperature and pressure (Fleet,
688 2017).
689
690 **Tables**
691 **Table 1.** Lattice parameters for A-type products. Uncertainty in lattice parameters obtained in this
692 study, ±0.001 Å.

Apatite	a-axis (Å)	c-axis (Å)	Ref.
C_ACaApOH	9.521	6.873	Fleet and Liu, 2007
	9.530	6.888	this work
CaApOH	9.424	6.879	Sudarsanan and Young, 1969
C_ASrApOH	9.864	7.264	this work
SrApOH	9.764	7.280	Kazin et al., 2012
	9.745	7.265	Jebri et al., 2013
C_{AB}NaSrApOH*	9.808	7.264	this work

* C_{AB}NaSrApOH contains 1.0 % Na

693
694 **Table 2.** IR carbonate (ν_3) band frequencies (cm^{-1}) obtained for CCaApOH using the six- band
695 model.
696

This is a preprint, the final version is subject to change, of the American Mineralogist (MSA)
Cite as Authors (Year) Title. American Mineralogist, in press.
DOI: https://doi.org/10.2138/am-2019-6800

697

Sample	A	A'	A	B	B	A'	ΔA	ΔA'	ΔB	%CO_3	%Na
77	1530	1493	1472	1449	1418	1397	58	96	31	10.5	1.88
77P	1541	1489	1465	1448	1414	1386	76	103	34	7.35	0.9
82	1537	1496	1471	1450	1420	1396	66	100	30	8.9	0.14
82P	1546	1500	1461	1451	1413	1404	85	96	38	4.1	0.037
33	1528	1493	1470	1444	1413	1390	58	103	31	19.85	3.9
33P	1532	1486	1458	1443	1409	1386	74	100	34	18.6	3.7
40	1520	1496	1480	1455	1416	1395	40	101	39	6	0.165
40P	1544	1505	1473	1448	1413	1384	71	121	35	7.25	1.44
41	1534	1495	1474	1451	1418	1395	60	100	33	6.2	0.042
41P	1540	1501	1462	1448	1417	1404	78	97	31	4.8	0.43
Averages	1535.2	1495.4	1468.6	1448.7	1415.1	1393.7	66.6	101.7	33.6		

698

699 **Table 3.** IR carbonate (ν_3) band frequencies (cm^{-1}) obtained for AB-CSrApOH using the four-
700 band model.

Apatite	A-type peaks		Δν	B-type peaks		Δν	wt% CO_3	wt% Na
44	1550	1443	107	1425	1402	23	4.6	0.33
44A	1544	1452	92	1427	1397	30	2.4	0.29
45	1549	1458	91	1434	1404	30	6.3	0.48
45A	1543	1454	89	no	no		4.6	0.27
34	1520	1462	58	1438	1408	30	6.9	0.89

This is a preprint, the final version is subject to change, of the American Mineralogist (MSA)
Cite as Authors (Year) Title. American Mineralogist, in press.
DOI: https://doi.org/10.2138/am-2019-6800

34A	1546	1458	88	1437	1405	32	6.6	1.00
62	1551	1457	94	1435	1409	26	5.0	0.45
62A	1546	1459	87	1440	1400	40	4.5	0.25
63	1551	1455	96	1433	1407	26	5.2	0.33
63A	1544	1453	91	1434	1395	39	5.5	0.04
Avg	1542	1454.5	87.5	1432	1403	29		

no = not observed

Table 4. A comparison of carbonate asymmetric stretch (ν_3) frequencies (cm^{-1}) of calcium apatites with low and high % A-type carbonate.

Apatite	% B-type*	A-type frequencies		B-type frequencies	
Mostly A-type					
82P	31	1546	1461	1451	1413
41P	24	1540	1462	1448	1417
Mostly B-type					
33P	97	1532	1458	1443	1409
77	92	1530	1472	1449	1418

* from a two band analysis of ν_2

Figures

This is a preprint, the final version is subject to change, of the American Mineralogist (MSA)
Cite as Authors (Year) Title. American Mineralogist, in press.
DOI: https://doi.org/10.2138/am-2019-6800

711
712

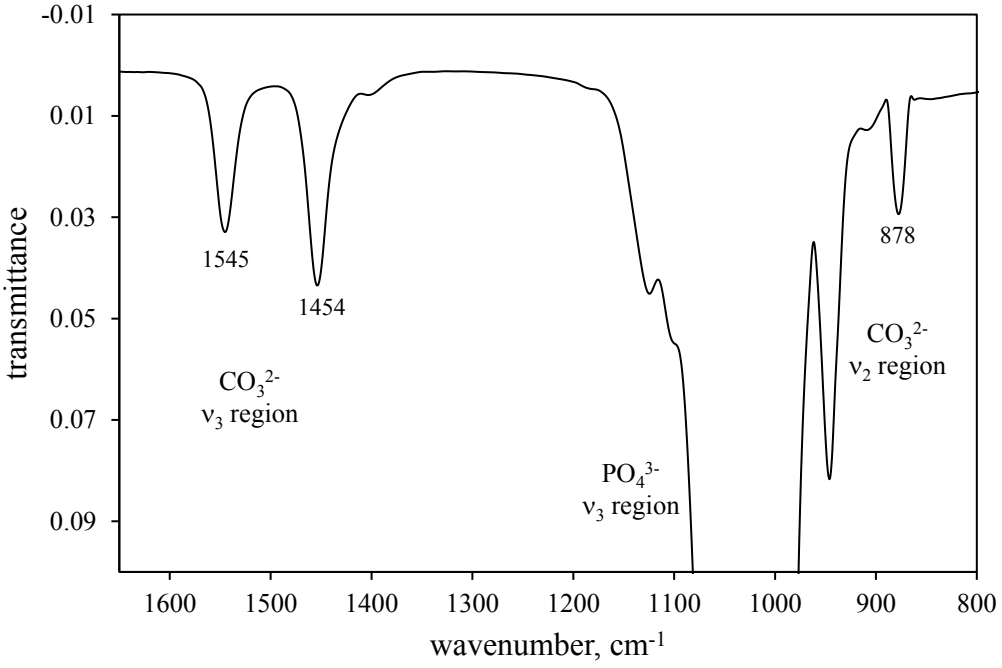

713
714 Figure 1
715

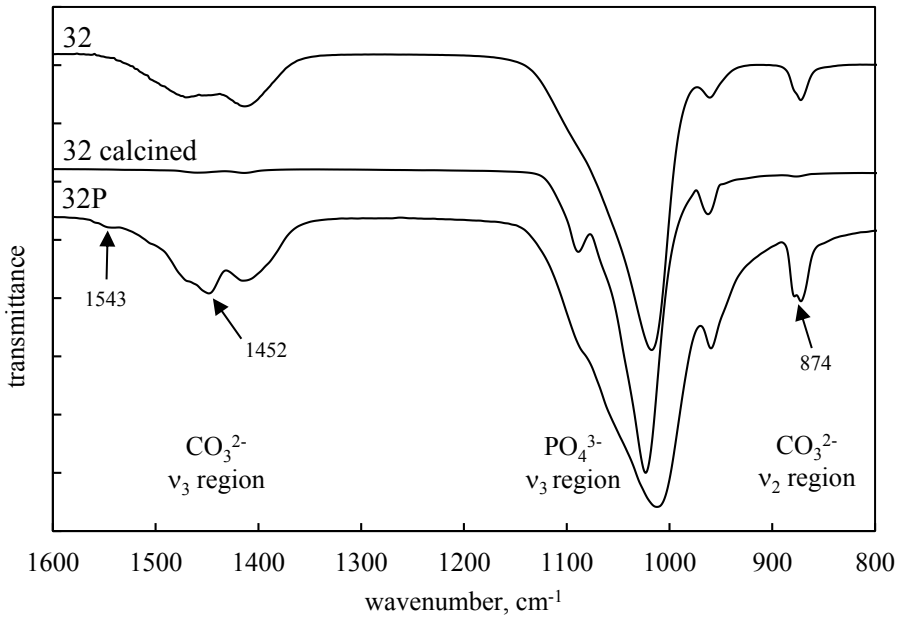

716
717 Figure 2
718

This is a preprint, the final version is subject to change, of the American Mineralogist (MSA)
Cite as Authors (Year) Title. American Mineralogist, in press.
DOI: https://doi.org/10.2138/am-2019-6800

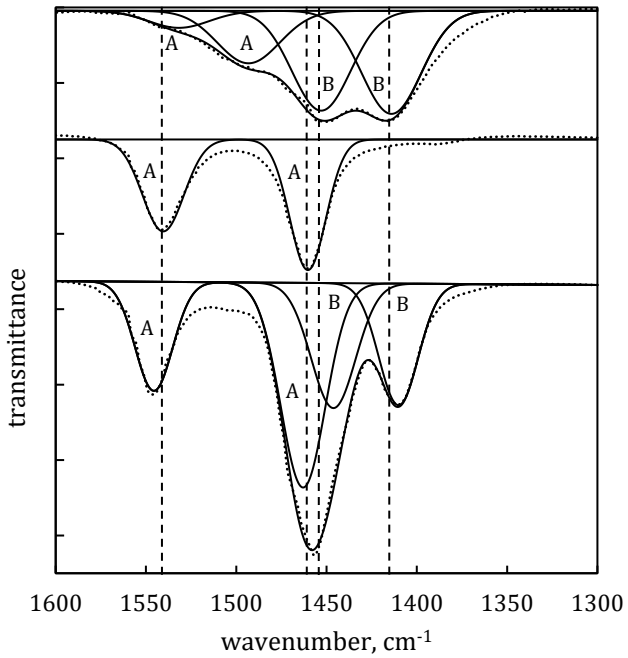

719

720 (a)

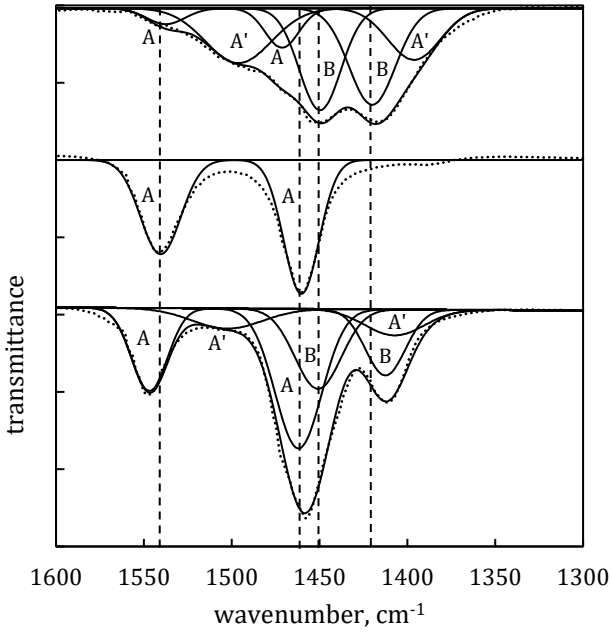

721

722 (b)

723 Figure 3
724

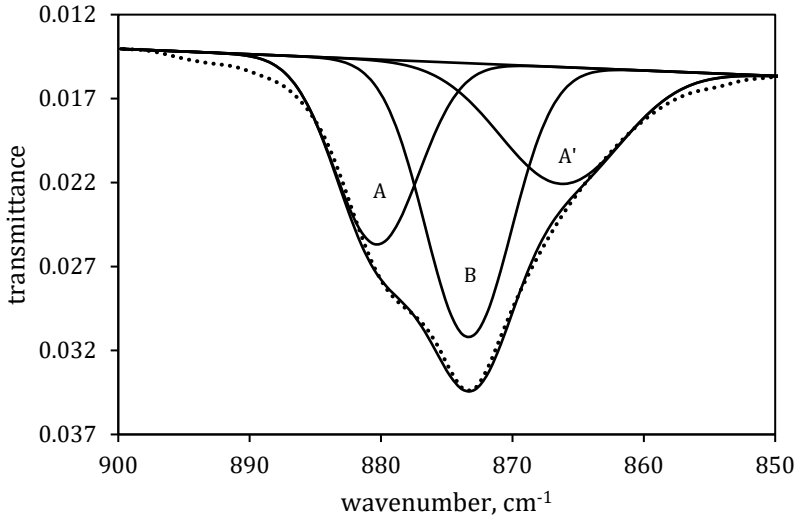

Figure 4

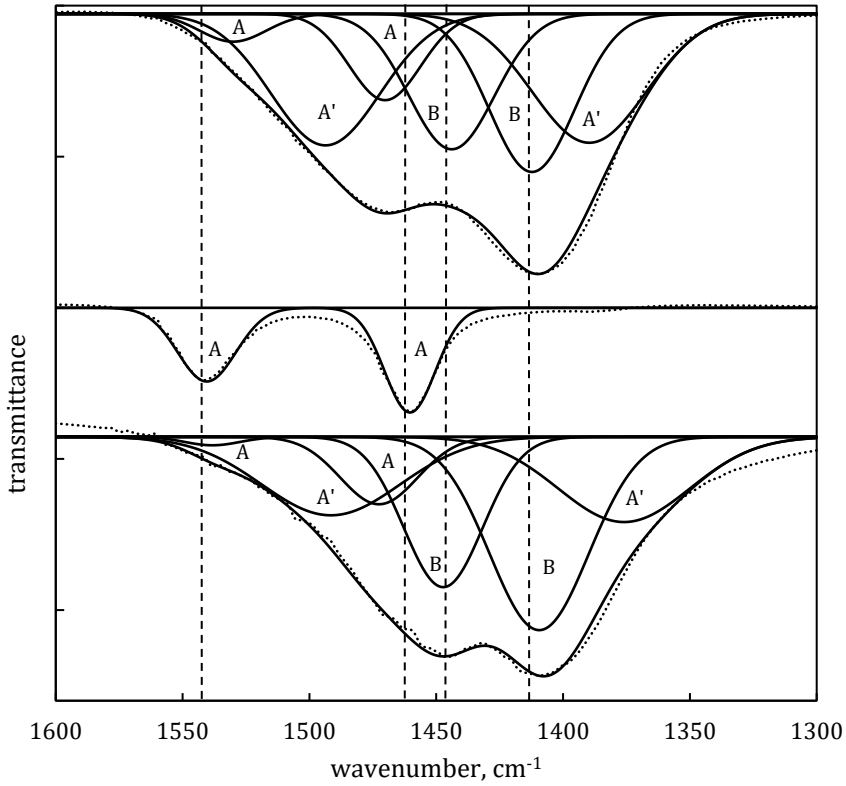

Figure 5

This is a preprint, the final version is subject to change, of the American Mineralogist (MSA)
Cite as Authors (Year) Title. American Mineralogist, in press.
DOI: https://doi.org/10.2138/am-2019-6800

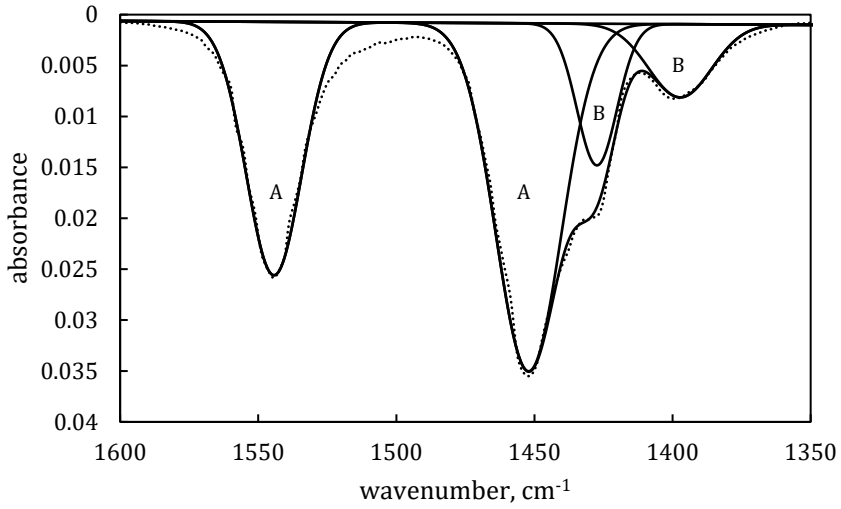

731
732 Figure 6

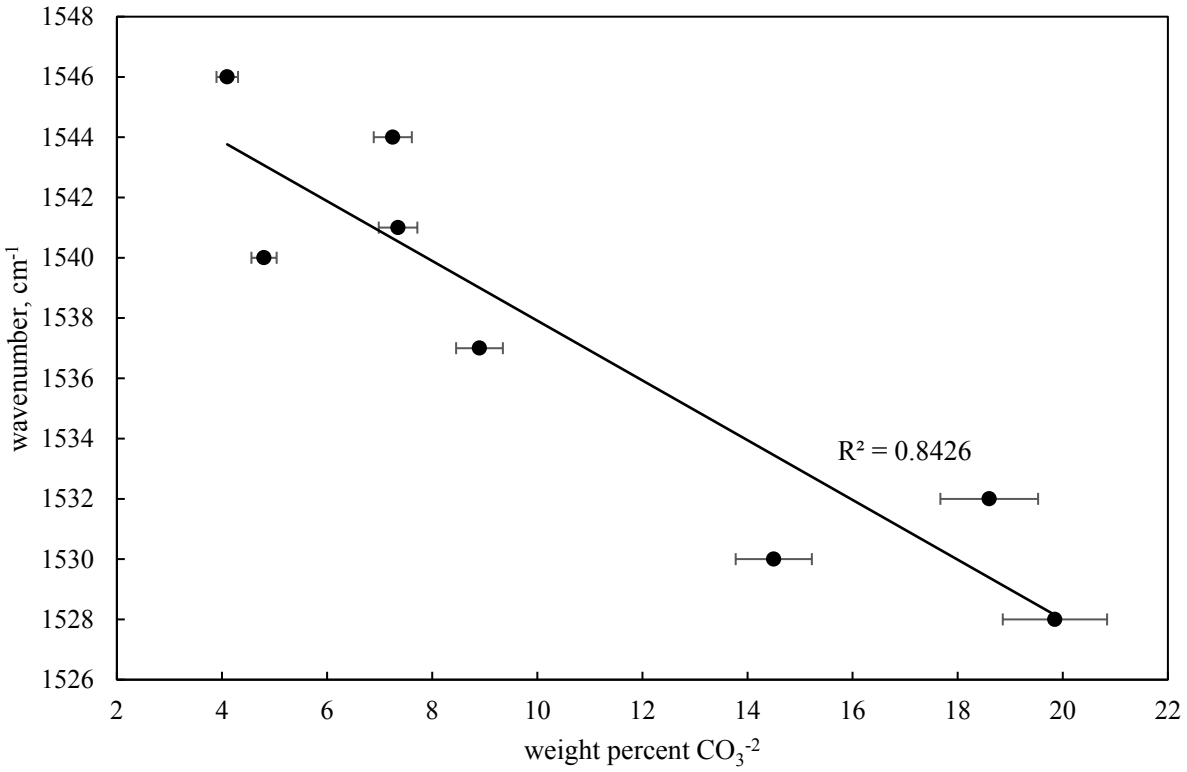

733
734 Figure 7
735

This is a preprint, the final version is subject to change, of the American Mineralogist (MSA)
Cite as Authors (Year) Title. American Mineralogist, in press.
DOI: https://doi.org/10.2138/am-2019-6800

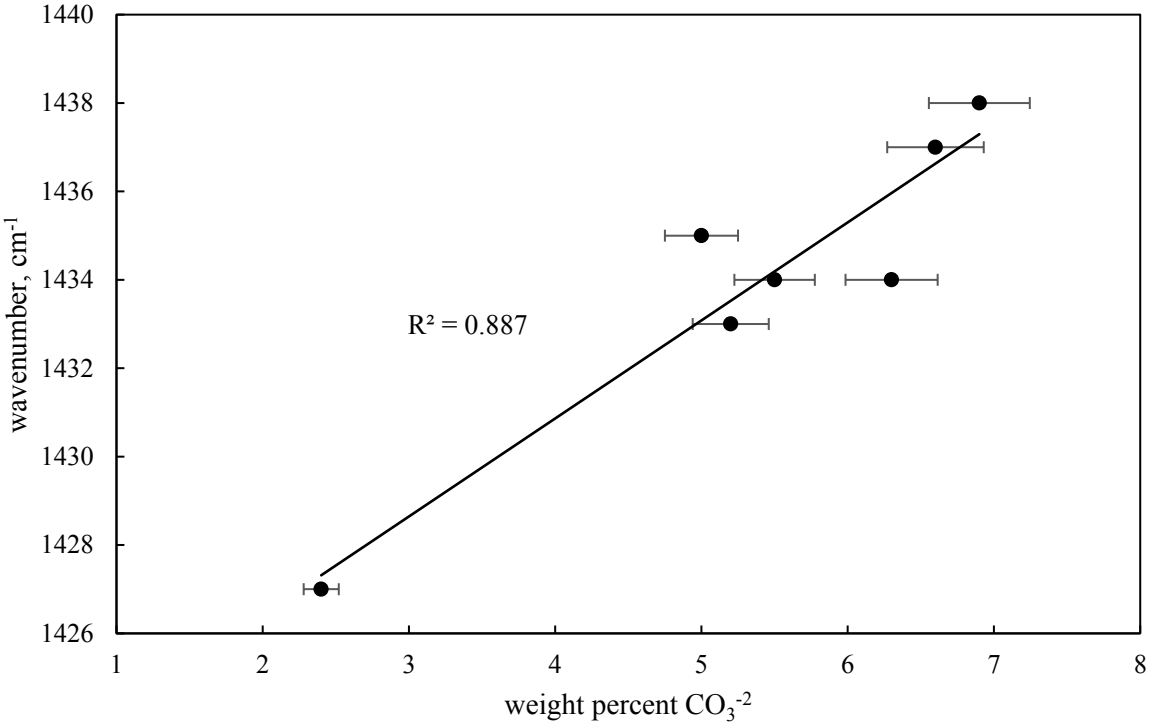

Figure 8

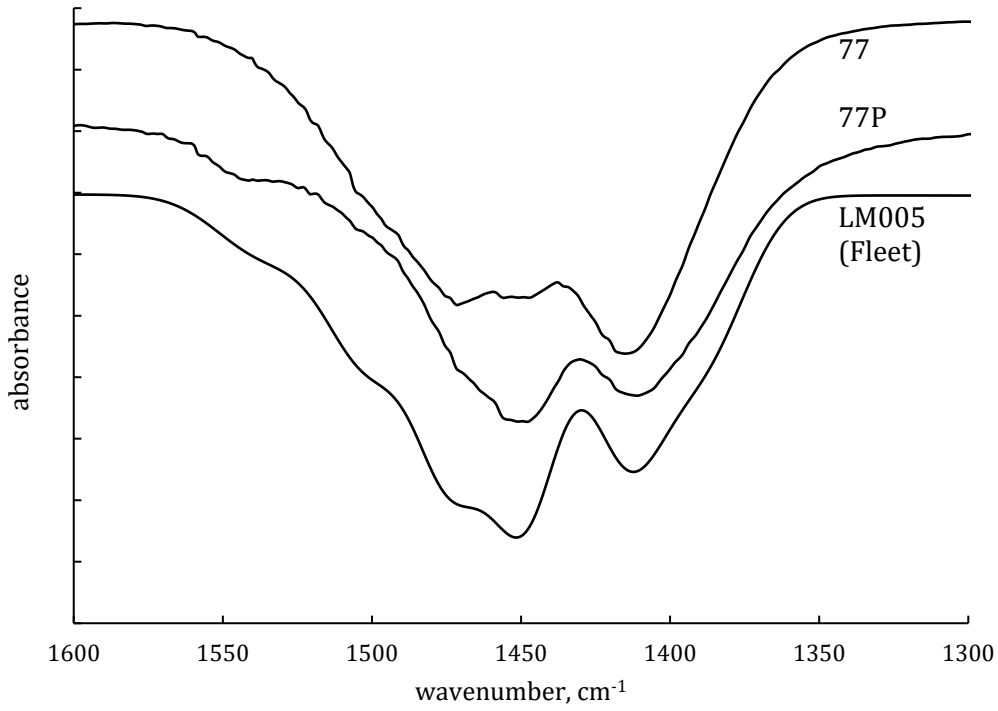

Figure 9